CHAPTER III

RESULTS AND DISCUSSION

The main purpose of this research is to study the relationship between electrochemical and the catalytic properties of catalysts responsible for the oxidation of cyclohexane to cyclohexanone and cyclohexanol. The metal Schiff base complexes were selected as a model to be examined by cyclic voltammatry.

3.1 Syntheses and characterization of metal Schiff base complexes

Five Schiff base ligands as shown below were synthesized by condensation reaction using aldehyde or ketone with appropriate primary diamines according to the literature procedure.[31] Their identities were well elucidated by IR and NMR techniques prior to use for synthesizing metal Schiff base complexes **(6)**-**(20)**. IR spectra of these complexes showed a characteristic absorption band in the range of 1630-1650 cm^{-1} attributable to azomethine group (C=N) vibration. For free ligands, this band occurs at higher frequencies ~ 10-15 cm^{-1} which was belonged to C=N.[32]

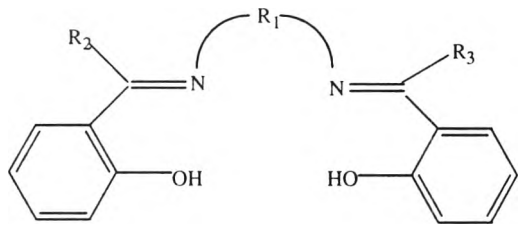

(1): $R_1 = C_6H_6$, $R_2 = H$, $R_3 = H$

(2) : $R_1 = C_2H_4$, $R_2 = H$, $R_3 = H$

(3) : $R_1 = C_2H_4$, $R_2 = CH_3$, $R_3 = CH_3$

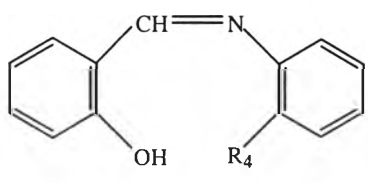

(4) : $R_4 = OH$

(5) : $R_4 = COOH$

3.2 Effect of metal-salophen complexes on reactivity of cyclohexane oxidation

The effect of metal complexes on the oxidation reaction was studied. The oxidation of cyclohexane was examined to observe both the rate of the reaction (observed at 2 h) and the amount of the desired products obtained (observed at 24 h). Seven metals, namely vanadium (as oxovanadium (IV)), copper (II), nickel (II), cobalt (II), chromium (III), manganese (II) and iron (II) were complexed with salophen **(1)** to gain metal Schiff base complexes **6-12**, respectively. The effects of various metal-salophen complexes on cyclohexane oxidation using H_2O_2 and TBHP are presented in Table 3.1.

Table 3.1 Cyclohexane oxidation catalyzed by various metal-salophen complexes

Catalysts	H_2O_2				TBHP			
	2 h		24 h		2 h		24 h	
	-one (mmol)	-ol (mmol)	-one (mmol)	-ol (mmol)	-one (mmol)	-ol (mmol)	-one (mmol)	-ol (mmol)
6	0	0	trace	0.507	0	0	trace	0.574
7	0	0	trace	trace	0.354	0.085	1.102	0.154
8	0	0	trace	trace	0	0	trace	trace
9	1.088	0.447	1.264	0.261	2.316	0.313	2.771	0.423
10	0.077	trace	0.098	trace	1.036	0.220	1.514	0.273
11	0	0	trace	trace	0	0	trace	trace
12	trace	trace	trace	trace	0.253	0.144	1.473	0.276

Reaction conditions: cyclohexane (30 mmol), metal-salophen complexes (0.25 mmol), pyridine and acetonitrile (1:1 V/V) (28 mL), H_2O_2 (15 mmol) at RT or TBHP (15 mmol) at 50 °C

From Table 3.1, it was observed that the reaction employing six metal-salophen complexes such as chromium **(7)**, copper **(8)**, iron **(9)**, manganese **(10)**, nickel **(11)** and oxovanadium **(12)** provided cyclohexanone as a major product and cyclohexanol being a minor while cobalt-salophen **(6)** gave an opposite result. Considering various metal salophen complexes, each gave different yield. Among them, metal complexes that provided good results in cyclohexane oxidation using both H_2O_2 and TBHP as an oxidant were iron (II), manganese (II) and vanadium (IV). Talking to the account of the effect of oxidant, TBHP was found to be relative inert when the reaction was carried out at room temperature. Nonetheless, when the oxidation was conducted at elevated temperature (50 °C), TBHP provided better yield of the desired products than H_2O_2 in all cases. The iron-salophen complex **(9)** still was a good catalyst in both conditions.

3.3 Effect of Schiff base structure on reactivity of cyclohexane oxidation

The effect of Schiff base on the oxidation reaction was focused. Five Schiff bases, namely salophen **(1)**, salen **(2)**, haen **(3)**, sap **(4)** and sac **(5)** were complexed with both oxovanadium (IV) and iron (II). All well-characterized complexes were employed as a catalyst in cyclohexane oxidation using both H_2O_2 and TBHP as an oxidant. The results are presented in Table 3.2 and Fig 3.1.

Table 3.2 Cyclohexane oxidation catalyzed by various metal Schiff base complexes

Catalysts	H_2O_2				TBHP			
	2 h		24 h		2 h		24 h	
	-one (mmol)	-ol (mmol)	-one (mmol)	-ol (mmol)	-one (mmol)	-ol (mmol)	-one (mmol)	-ol (mmol)
oxovanadium (IV) Schiff base complexes								
12	trace	trace	trace	trace	0.253	0.144	1.473	0.276
13	trace	trace	trace	trace	0.185	0.101	1.118	0.178
14	0	0	trace	trace	trace	trace	0.458	0.129
15	trace	trace	trace	trace	0.204	0.120	1.225	0.193
16	trace	trace	trace	trace	0.263	0.155	1.492	0.415
iron (II) Schiff base complexes								
9	1.088	0.447	1.264	0.261	2.316	0.313	2.771	0.423
17	0.986	0.396	1.418	0.249	2.451	0.286	2.527	0.320
18	0	0	trace	trace	trace	trace	1.395	0.213
19	0.343	0.258	0.716	0.426	0.814	0.199	1.516	0.216
20	1.640	0.489	1.815	0.356	2.700	0.309	2.851	0.546

Reaction conditions: cyclohexane (30 mmol), catalyst (0.25 mmol), pyridine and acetonitrile (1:1 V/V) (28 mL), H_2O_2 (15 mmol) at RT or TBHP (15 mmol) at 50 °C

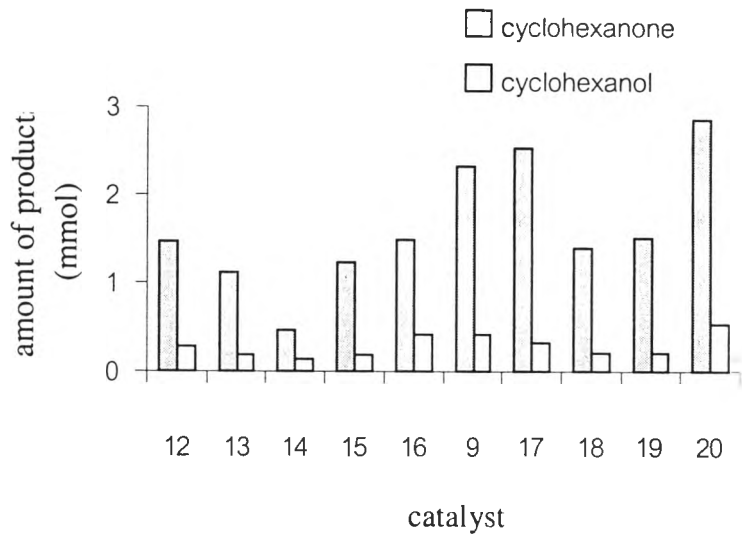

Fig 3.1 Effect of various metal Schiff base complexes in cyclohexane oxidation

From Table 3.2 and Fig 3.1, it was found that cyclohexanone was produced as a major product while cyclohexanol being a minor in all cases. Considering iron and oxovanadium Schiff base complexes, Schiff base that comprised electron withdrawing group and aromatic moiety provided good results namely **1**, **2**, **4** and **5**. In addition, the results derived from the reactions using H_2O_2 as oxidant was in good agreement with those employing TBHP as oxidant. However, the yield of using TBHP as oxidant was higher than H_2O_2 as oxidant.

3.4 Analysis of the redox reaction of metal Schiff base complexes by cyclic voltammetry

Electrochemical techniques can be used for following the progress of the reaction. These processes take place at the electrode-solution interface by fitting the substrate at the surface of electrode. Cyclic voltammetry, one of the electrochemical techniques is the most effective and versatile electroanalytical technique available for the mechanistic study of redox systems. This technique can be used for studying the

relationship between the current and the potential by rapidly scanned a potential. In this research, the redox property of metal Schiff base complexes was examined by cyclic voltammetry using both glassy carbon and boron-doped diamond electrodes as a working electrode, silver wire as a reference electrode and platinum wire as an auxillary electrode.

3.4.1 Study the redox reaction using glassy carbon as a working electrode

Two working electrodes: glassy carbon electrode and boron-doped diamond electrode were selected for comparative study of the electrochemical properties. Glassy carbon electrode is a carbon electrode. The microstructures consist of layers of condensed, six-membered aromatic rings with sp^2-hybridized carbon atom trigonally bonded to one another.[33] The cyclic voltammograms of metal Schiff base complexes examined by using glassy carbon electrode and voltage scan rate at 0.05 V/s are presented in Figs 3.2-3.13 and Table 3.3.

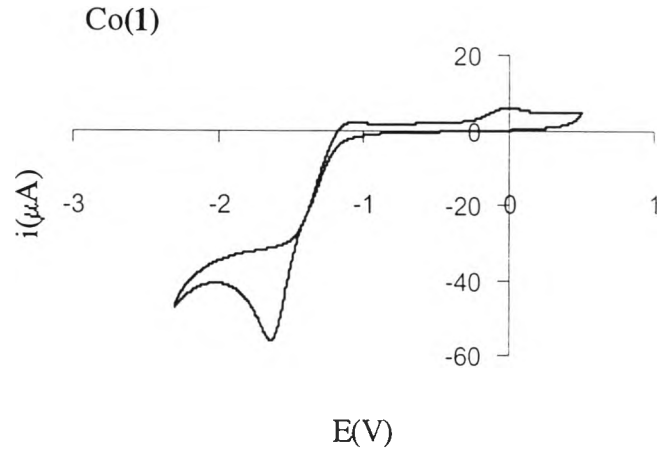

Fig 3.2 Cyclic voltammogram of complex **6** in 0.1 M $C_{16}H_{36}FNP$ obtained from using glassy carbon as working electrode, scan rate: 0.05 V/s

From Fig 3.2, complex **6** showed the peak potential separation of ΔE_p = 1.666 V which was larger than the 0.059 V anticipated for quasi-reversible reduction one-electron transfer at -1.641 V versus silver wire.

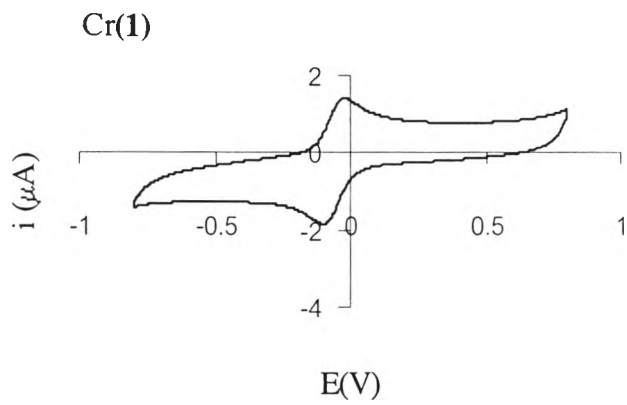

Fig 3.3 Cyclic voltammogram of complex **7** in 0.1 M $C_{16}H_{36}FNP$ obtained from using glassy carbon as working electrode, scan rate: 0.05 V/s

From Fig 3.3, complex **7** showed the peak current ratio i_{pa}/i_{pc} was nearly equal to unity and the peak potential separation of ΔE_p = 0.080 V which was only slightly larger than the 0.059 V anticipated for reversible reduction one-electron transfer at –0.101 V versus silver wire.

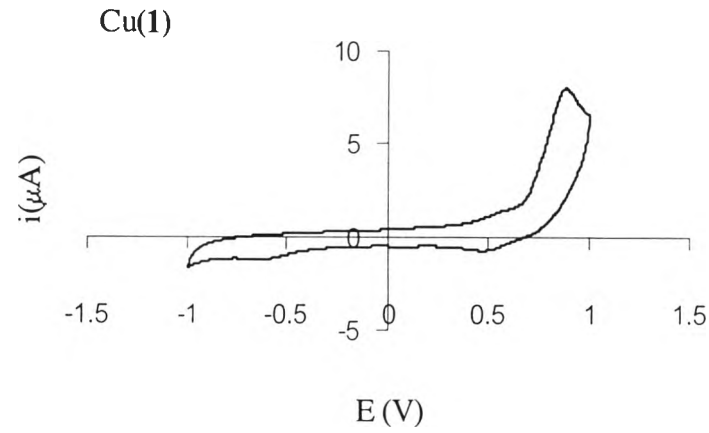

Fig 3.4 Cyclic voltammogram of complex **8** in 0.1 M $C_{16}H_{36}FNP$ obtained from using glassy carbon as working electrode, scan rate: 0.05 V/s

From Fig 3.4, complex **8** showed the oxidation peak at 0.885 V versus silver wire which was anticipated for irreversible oxidation one-electron transfer.

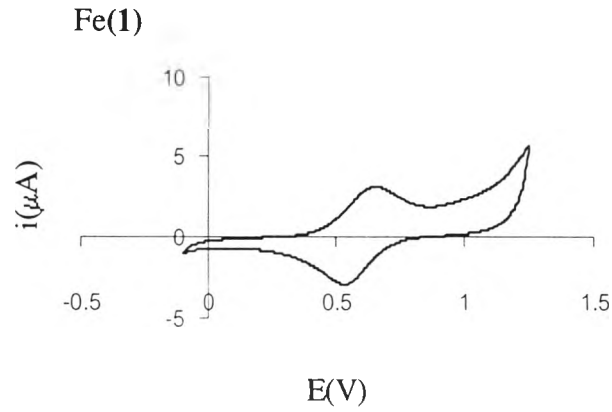

Fig 3.5 Cyclic voltammogram of complex **9** in 0.1 M $C_{16}H_{36}FNP$ obtained from using glassy carbon as working electrode, scan rate: 0.05 V/s

From Fig 3.5, complex **9** showed the peak current ratio i_{pa}/i_{pc} was nearly equal to unity and the peak potential separation of ΔE_p = 0.098 V which was only slightly larger than the 0.059 V anticipated for reversible reduction one-electron transfer at 0.553 V versus silver wire.

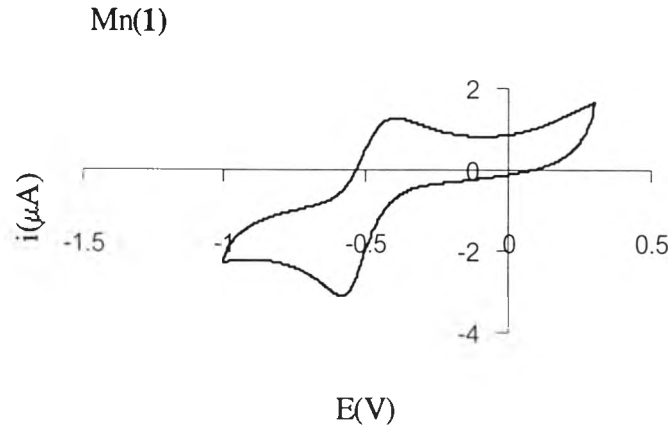

Fig 3.6 Cyclic voltammogram of complex **10** in 0.1 M $C_{16}H_{36}FNP$ obtained from using glassy carbon as working electrode, scan rate: 0.05 V/s

From Fig 3.6, complex **10** showed the peak potential separation of ΔE_p = 0.204 V which was larger than the 0.059 V anticipated for quasi-reversible reduction one-electron transfer at –0.601 V versus silver wire.

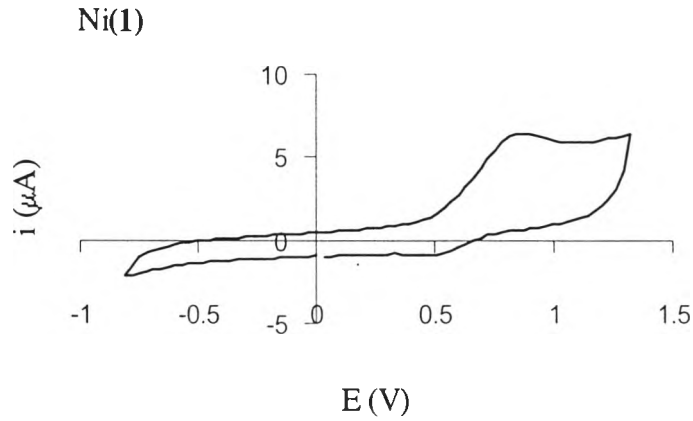

Fig 3.7 Cyclic voltammogram of complex **11** in 0.1 M $C_{16}H_{36}FNP$ obtained from using glassy carbon as working electrode, scan rate: 0.05 V/s

From Fig 3.7, complex **11** showed the oxidation peak at 0.872 V versus silver wire which was anticipated for irreversible oxidation one-electron transfer.

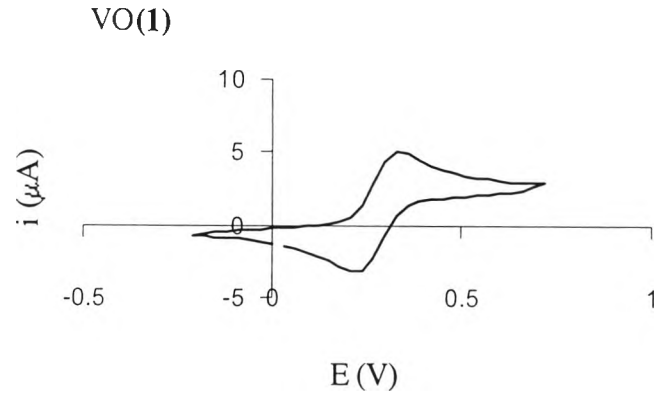

Fig 3.8 Cyclic voltammogram of complex **12** in 0.1 M $C_{16}H_{36}FNP$ obtained from using glassy carbon as working electrode, scan rate: 0.05 V/s

From Fig 3.8, complex **12** showed the peak current ratio i_{pa}/i_{pc} was nearly equal to unity and the peak potential separation of ΔE_p = 0.091 V which was only slightly larger than the 0.059 V anticipated for reversible reduction one-electron transfer at 0.240 V versus silver wire.

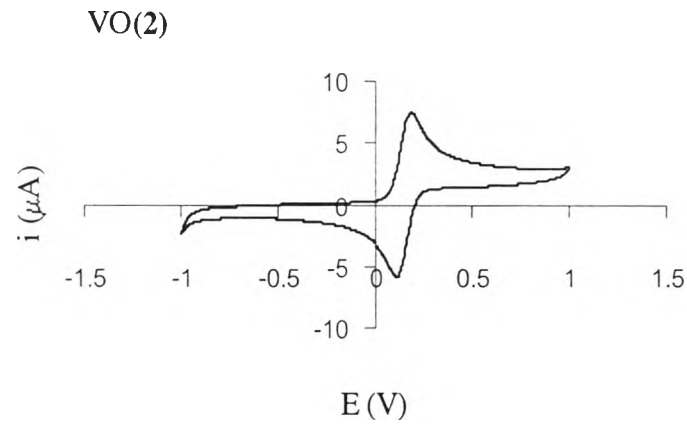

Fig 3.9 Cyclic voltammogram of complex **13** in 0.1 M $C_{16}H_{36}FNP$ obtained from using glassy carbon as working electrode, scan rate: 0.05 V/s

From Fig 3.9, complex **13** showed the peak current ratio i_{pa}/i_{pc} was nearly equal to unity and the peak potential separation of ΔE_p = 0.076 V which was only slightly larger than the 0.059 V anticipated for reversible reduction one-electron transfer at 0.113 V versus silver wire.

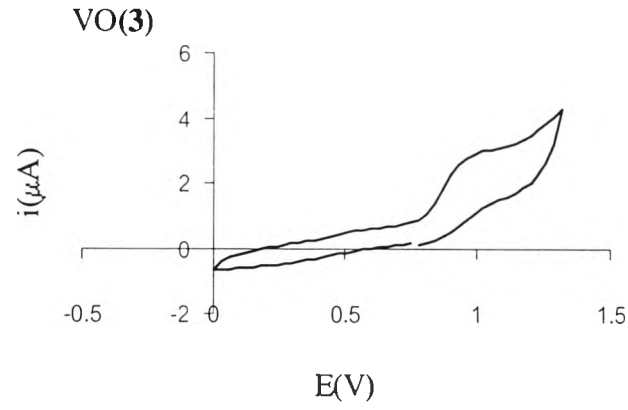

Fig 3.10 Cyclic voltammogram of complex **14** in 0.1 M $C_{16}H_{36}FNP$ obtained from using glassy carbon as working electrode, scan rate: 0.05 V/s

From Fig 3.10, complex **14** showed the oxidation peak at 1.021 V versus silver wire which was anticipated for irreversible oxidation one-electron transfer.

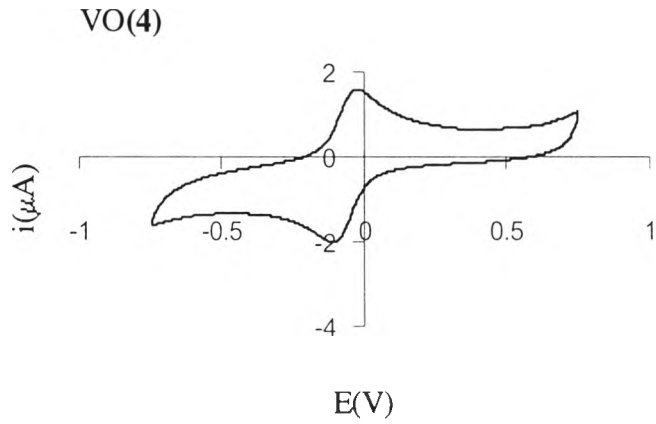

Fig 3.11 Cyclic voltammogram of complex **15** in 0.1 M $C_{16}H_{36}FNP$ obtained from using glassy carbon as working electrode, scan rate: 0.05 V/s

From Fig 3.11, complex **15** showed the peak current ratio i_{pa}/i_{pc} was nearly equal to unity and the peak potential separation of ΔE_p = 0.076 V which was only slightly larger than the 0.059 V anticipated for reversible reduction one-electron transfer at -0.131 V versus silver wire.

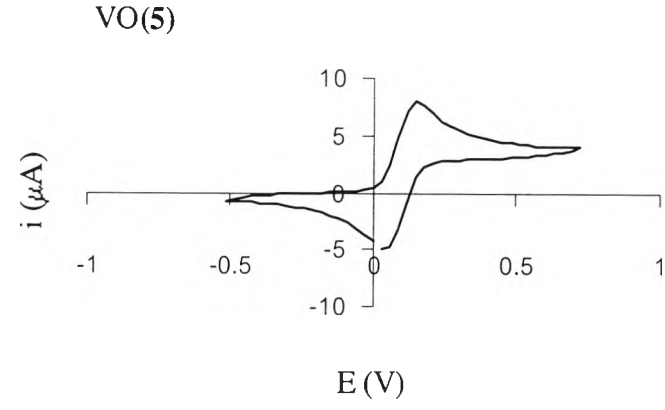

Fig 3.12 Cyclic voltammogram of complex **16** in 0.1 M $C_{16}H_{36}FNP$ obtained from using glassy carbon as working electrode, scan rate: 0.05 V/s

From Fig 3.12, complex **16** showed the peak current ratio i_{pa}/i_{pc} was nearly equal to unity and the peak potential separation of ΔE_p = 0.080 V which was only slightly larger than the 0.059 V anticipated for reversible reduction one-electron transfer at 0.070 V versus silver wire.

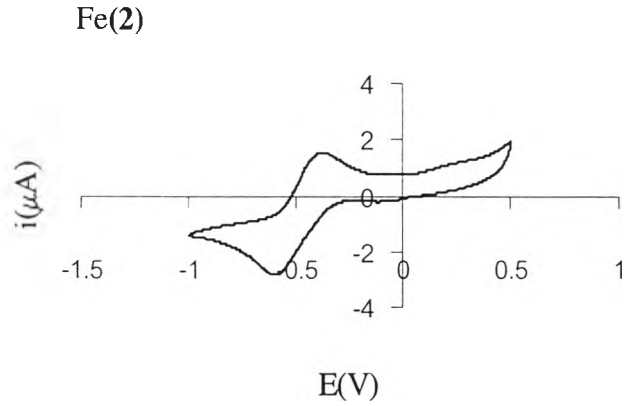

Fig 3.13 Cyclic voltammogram of complex **17** in 0.1 M $C_{16}H_{36}FNP$ obtained from using glassy carbon as working electrode, scan rate: 0.05 V/s

From Fig 3.13, complex **17** showed the peak potential separation of ΔE_p = 0.104 V which was larger than the 0.059 V anticipated for quasi-reversible reduction one-electron transfer at –0.629 V versus silver wire.

Table 3.3 The redox property of metal Schiff base complexes using a glassy carbon electrode

Catalysts		E_{pc}	i_{pc}	E_{pa}	i_{pa}	E_{pa}-E_{pc} (ΔE_p)	Redox reaction
Co(**1**)	**6**	-1.641	-56.152	0.025	5.823	1.666	Quasi-reversible
Cr(**1**)	**7**	-0.101	-1.852	-0.021	1.402	0.080	Reversible
Cu(**1**)	**8**	-	-	0.885	7.980	-	Irreversible
Fe(**1**)	**9**	0.553	-2.732	0.651	2.945	0.098	Reversible
Mn(**1**)	**10**	-0.601	-3.066	-0.397	1.258	0.204	Quasi-reversible
Ni(**1**)	**11**	-	-	0.872	6.443	-	Irreversible
VO(**1**)	**12**	0.240	-4.200	0.331	4.967	0.091	Reversible
VO(**2**)	**13**	0.113	-5.853	0.189	7.049	0.076	Reversible
VO(**3**)	**14**	-	-	1.021	2.988	-	Irreversible
VO(**4**)	**15**	-0.131	-1.955	-0.055	1.578	0.076	Reversible
VO(**5**)	**16**	0.070	-5.032	0.150	6.944	0.080	Reversible
Fe(**2**)	**17**	-0.589	-2.455	-0.385	1.668	0.104	Quasi-reversible

Recorded for 0.1 mM solutions of complexes in 0.1 M $C_{16}H_{36}FNP$ using a glassy carbon electrode vs silver wire reference electrode; CV sweep rate 0.05 V/s

The cyclic voltammogram was characterized by several important parameters to inform the kinds of redox reactions. The reversible process exhibited the ΔE_p value about 0.059 V and the ratio of i_{pa} to i_{pc} is unity. The quasi-reversible displayed the ΔE_p value more than 0.059 V, for irreversible process, the individual peak was reduced in size and widely separated.

From Figs. 3.2-3.13 and Table 3.4, it was found that complexes **7**, **9**, **12**, **13**, **15** and **16** showed the ΔE_p value close to 0.059 V and the values of i_{pa} and i_{pc} were close to a reported reversible reaction[8]; thus it should be a reversible process. Considering the ΔE_p value, the ΔE_p value of complexes **7**, **9**, **12**, **13**, **15** and **16** were more than 0.059 V because of the ohmic (iR) drop occurred by effect of solution resistance. The metal Schiff base complexes **6, 10** and **17** revealed the ΔE_p value more than 0.059 V exhibiting quasi-reversible reactions. The metal Schiff base complexes **8**, **11** and **14** showed the only oxidation peak demonstrating irreversible reactions. However, these three metal Schiff base complexes **18**, **19** and **20** were not soluble in the reaction media and thus their redox properties could not be examined.

3.4.2 Study the redox reaction using boron-doped diamond electrode as working electrode

Boron-doped diamond electrode consists of a diamond doped with boron using hot-filament. This material possesses semimetal electronic properties, making it useful for electrochemical measurements.[34] The cyclic voltammogram of metal Schiff base complexes was examined using boron-doped diamond as a working electrode and voltage scan rate at 0.05 V/s are presented in Figs 3.14-3.25 and Table 3.4.

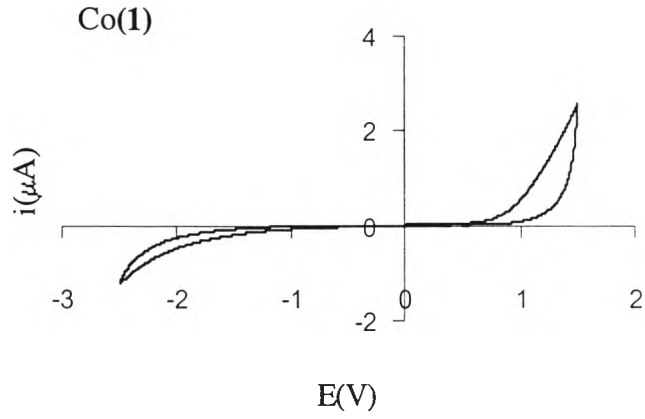

Fig 3.14 Cyclic voltammogram of complex **6** in 0.1 M $C_{16}H_{36}FNP$ obtained from using boron-doped diamond as working electrode, scan rate: 0.05 V/s

From Fig 3.14, complex **6** did not show redox reaction .

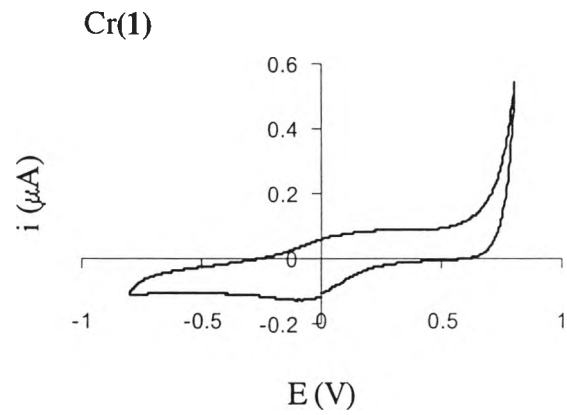

Fig 3.15 Cyclic voltammogram of complex **7** in 0.1 M $C_{16}H_{36}FNP$ obtained from using boron-doped diamond as working electrode, scan rate: 0.05 V/s

From Fig 3.15, complex **7** did not show redox reaction.

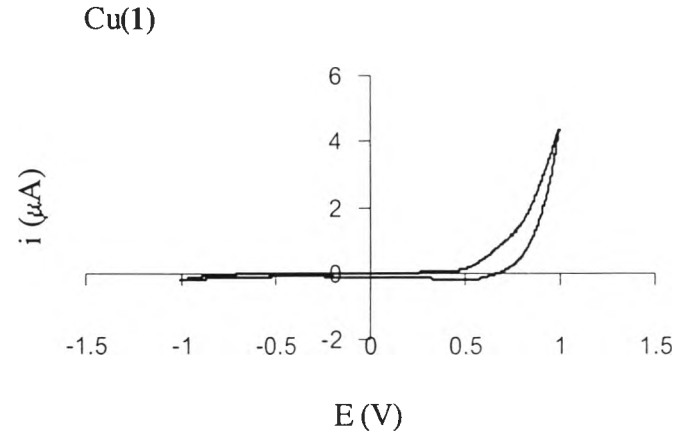

Fig 3.16 Cyclic voltammogram of complex **8** in 0.1 M $C_{16}H_{36}FNP$ obtained from using boron-doped diamond as working electrode, scan rate: 0.05 V/s

From Fig 3.16, complex **8** did not show redox reaction.

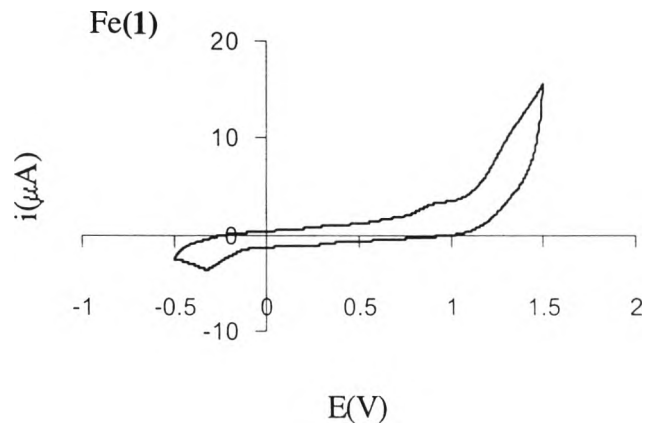

Fig 3.17 Cyclic voltammogram of complex **9** in 0.1 M $C_{16}H_{36}FNP$ obtained from using boron-doped diamond as working electrode, scan rate: 0.05 V/s

From Fig 3.17, complex **9** showed the reduction peak at –0.373 V versus silver wire which was anticipated for irreversible reduction one-electron transfer.

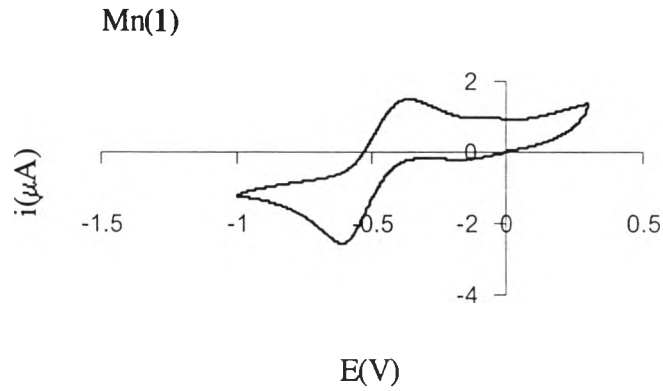

Fig 3.18 Cyclic voltammogram of complex **10** in 0.1 M $C_{16}H_{36}FNP$ obtained from using boron-doped diamond as working electrode, scan rate: 0.05 V/s

From Fig 3.18, complex **10** showed the peak potential separation of ΔE_p = 0.284 V which was larger than the 0.059 V anticipated for quasi-reversible reduction one-electron transfer at –0.638 V versus silver wire.

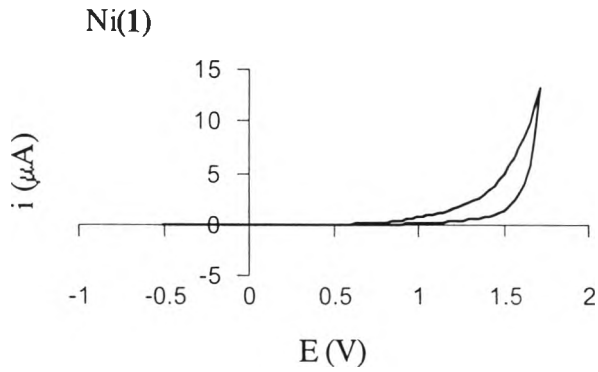

Fig 3.19 Cyclic voltammogram of complex **11** in 0.1 M $C_{16}H_{36}FNP$ obtained from using boron-doped diamond as working electrode, scan rate: 0.05 V/s

From Fig 3.19, complex **11** did not show redox reaction.

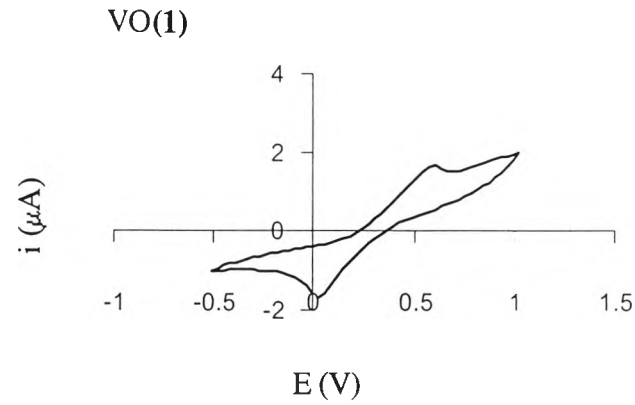

Fig 3.20 Cyclic voltammogram of complex **12** in 0.1 M $C_{16}H_{36}FNP$ obtained from using boron-doped diamond as working electrode, Scan rate: 0.05 V/s

From Fig 3.20, complex **12** showed the peak current ratio i_{pa}/i_{pc} was nearly equal to unity and the peak potential separation of ΔE_p = 0.571 V which was a lot larger than the 0.059 V anticipated for quasi-reversible reduction one-electron transfer at 0.030 V versus silver wire.

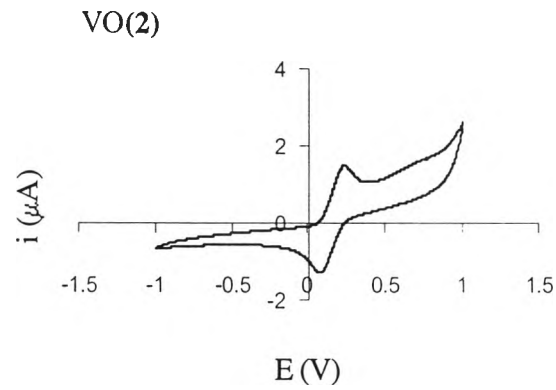

Fig 3.21 Cyclic voltammogram of complex **13** in 0.1 M $C_{16}H_{36}FNP$ obtained from using boron-doped diamond as working electrode, Scan rate: 0.05 V/s

From Fig 3.21, complex **13** showed the peak current ratio i_{pa}/i_{pc} was nearly equal to unity and the peak potential separation of ΔE_p = 0.090 V which was only slightly larger than the 0.059 V anticipated for reversible reduction one-electron transfer at 0.139 V versus silver wire.

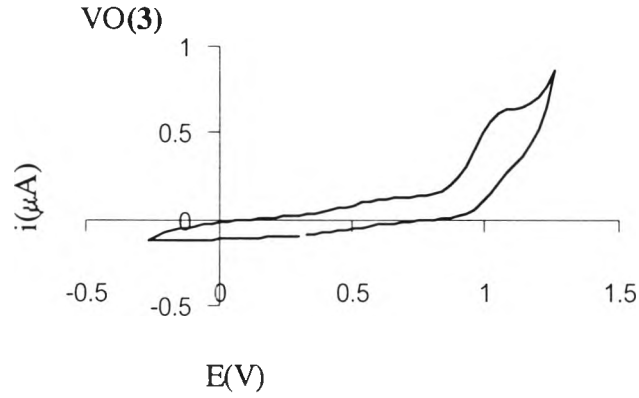

Fig 3.22 Cyclic voltammogram of complex **14** in 0.1 M $C_{16}H_{36}FNP$ obtained from using boron-doped diamond as working electrode, scan rate: 0.05 V/s

From Fig 3.22, complex **14** showed the oxidation peak at 1.142 V versus silver wire which was anticipated for irreversible oxidation one-electron transfer.

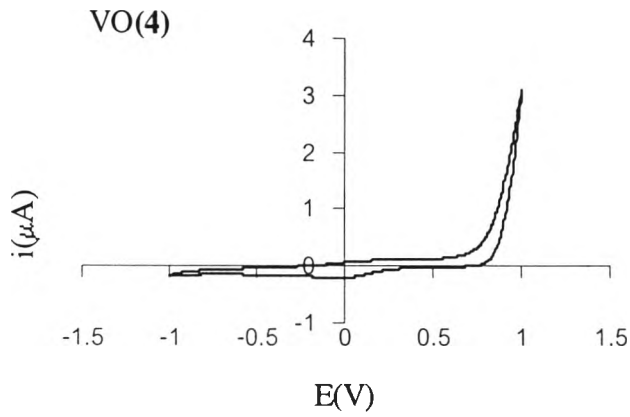

Fig 3.23 Cyclic voltammogram of complex **15** in 0.1 M $C_{16}H_{36}FNP$ obtained from using boron-doped diamond as working electrode, scan rate: 0.05 V/s

From Fig 3.23, complex **15** did not show redox reaction.

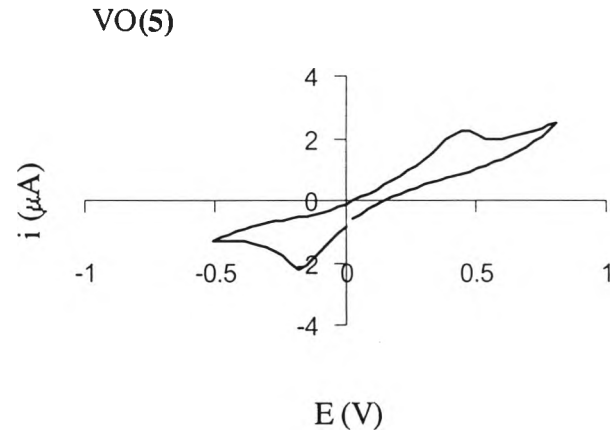

Fig 3.24 Cyclic voltammogram of complex **16** in 0.1 M $C_{16}H_{36}FNP$ obtained from using boron-doped diamond as working electrode, Scan rate: 0.05 V/s

From Fig 3.24, complex **16** showed the peak current ratio i_{pa}/i_{pc} was nearly equal to unity and the peak potential separation of ΔE_p = 0.661 V which was a lot larger than the 0.059 V anticipated for quasi-reversible reduction one-electron transfer at-0.180 V versus silver wire.

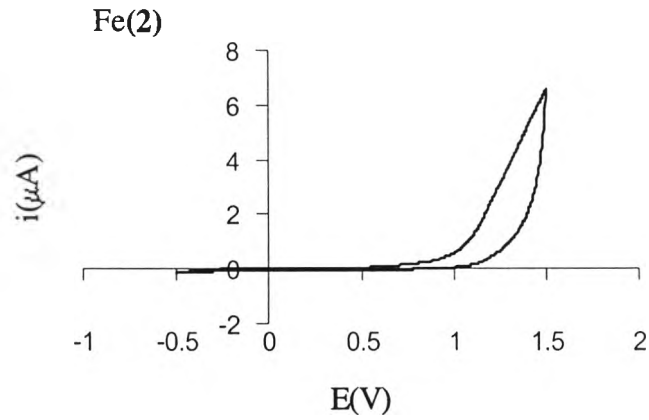

Fig 3.25 Cyclic voltammogram of complex **17** in 0.1 M $C_{16}H_{36}FNP$ obtained from using boron-doped diamond as working electrode, scan rate: 0.05 V/s

From Fig 3.25, complex **17** did not show redox reaction.

Table 3.4 The redox property of metal Schiff base complexes using boron-doped diamond as a working electrode

Catalysts		E_{pc}	i_{pc}	E_{pa}	i_{pa}	E_{pa}-E_{pc} (ΔE_p)	Redox reaction
Co(**1**)	**6**	-	-	-	-	-	-
Cr(**1**)	**7**	-	-	-	-	-	-
Cu(**1**)	**8**	-	-	-	-	-	-
Fe(**1**)	**9**	-0.373	-3.348	-	-	-	Irreversible
Mn(**1**)	**10**	-0.638	-2.476	-0.354	1.481	0.284	Quasi-reversible
Ni(**1**)	**11**	-	-	-	-	-	-
VO(**1**)	**12**	0.030	-1.697	0.601	1.666	0.571	Quasi-reversible
VO(**2**)	**13**	0.139	-1.264	0.229	1.583	0.090	Reversible
VO(**3**)	**14**	-	-	1.142	0.643	-	Irreversible
VO(**4**)	**15**	-	-	-	-	-	-
VO(**5**)	**16**	-0.180	-2.204	0.481	2.225	0.661	Quasi-reversible
Fe(**2**)	**17**	-	-	-	-	-	-

Recorded for 0.1 mM solutions of complexes in 0.1 M $C_{16}H_{36}FNP$ using a boron-doped diamond electrode vs silver wire reference electrode; CV sweep rate 0.05 V/s.

From Figs. 3.14-3.25 and Table 3.4, it was found that complexes **13** showed the ΔE_p value close to 0.059 V. The values of i_{pa} and i_{pc} are similar to a reported reversible reaction; thus it should be a reversible process. Considering the ΔE_p value, the ΔE_p value was more than 0.059 V because of the ohmic (iR) drop occurred by effect of the solution resistance. The metal Schiff base complex **10**, **12** and **16** showed the ΔE_p value more than 0.059 V exhibiting quasi-reversible reactions. While

complexes **9** showed the only reduction peak and complex **14** showed the only oxidation peak displayed irreversible reactions. The metal Schiff base complexes **6**, **7**, **8**, **11**, **15** and **17** did not reveal redox property. The metal Schiff base complexes **18**, **19** and **20** were not well soluble in the reaction media. Thus, their redox properties could not be examined.

3.5 Comparative study of the redox property using glassy carbon and boron-doped diamond electrodes as a working electrodes

There are several interesting electroanalytically important properties that can be used to distinguish boron-doped diamond from a conventional carbon electrode. The boron-doped diamond electrode would exhibit voltammetric background currents and double-layer capacitances up to an order of magnitude lower than for that of glassy carbon and exhibited a wide working potential window for solvent-electrolyte electrolysis more than glassy carbon electeode.[35, 36] In this research, glassy carbon and boron-doped diamond electrodes were employed as working electrode for comparison the redox property of the metal Schiff base complexes.

From Figs 3.2-3.13 and Table 3.3 and Figs 3.14-3.25 and Table 3.4, it could be noticed that the redox property result obtained from using glassy carbon and boron-doped diamond electrodes as working electrode were different. Considering the ΔE_p value of complexes **13** possessing reversible reaction, that of complex **13** for boron-doped diamond electrode was notably larger than that glassy carbon electrode. This was because the electrode-reaction kinetic of boron-doped diamond electrode was slow.[37] Thus, the difference of redox property results for the other metal Schiff base complexes could be implied by the same reason.

3.6 Comparative redox and catalytic properties of metal Schiff base complexes

One of the main goals of this research is to study the relationship between electrochemical and catalytic properties of metal Schiff base complexes. The outcome from this study would be a benefit for the selection of appropriate catalyst. The results of catalytic and redox properties are summarized in Table 3.5.

Table 3.5 The catalytic and redox properties of the metal Schiff base complexes

Catalysts		Product (mmol)		Redox reaction (obtained from glassy carbon electrode)
		-one	-ol	
Co(**1**)	**6**	trace	0.574	Quasi-reversible
Cr(**1**)	**7**	1.102	0.154	Reversible
Cu(**1**)	**8**	trace	trace	Irreversible
Fe(**1**)	**9**	2.316	0.423	Reversible
Mn(**1**)	**10**	1.514	0.273	Quasi-Reversible
Ni(**1**)	**11**	trace	trace	Irreversible
VO(**1**)	**12**	1.473	0.276	Reversible
VO(**2**)	**13**	1.118	0.178	Reversible
VO(**3**)	**14**	0.458	0.129	Irreversible
VO(**4**)	**15**	1.225	0.193	Reversible
VO(**5**)	**16**	1.492	0.415	Reversible
Fe(**2**)	**17**	2.527	0.320	Quasi-reversible

(1) : salophen **(2)** : salen **(3)** : hean **(4)** : sap **(5)** : sac

From Table 3.5, it was found that complexes **7**, **9**, **12, 13, 15, 16, 10** and **17** provided the product yield better than other complexes. These complexes exhibited the

reversible reaction and quasi-reversible, respectively. Complex **6** provided cyclohexanol as a main product and showed the quasi-reversible reaction. This was because the cathodic peak of quasi-reversible was more stable than the anodic peak. While complexes **8, 11** and **14** gave trace amount of desired product displayed an irreversible reaction. Therefore, it could clearly be seen that metal Schiff base complexes gave the catalytic property result in concomitant with that of redox property.

3.7 Kinetic study on the reaction rate of cyclohexane oxidation

The kinetic study of reaction was performed for finding appropriate time to observe the progress of the reaction. The rate of cyclohexane oxidation catalyzed by complexes **9**, **10** and **12** using TBHP as oxidant was studied.

3.7.1 Kinetic study of cyclohexane oxidation

The kinetic study of cyclohexane oxidation using complexes **9, 10** and **12** as catalyst and TBHP as oxidant was carried out. The kinetic analysis results are presented in Fig 3.26.

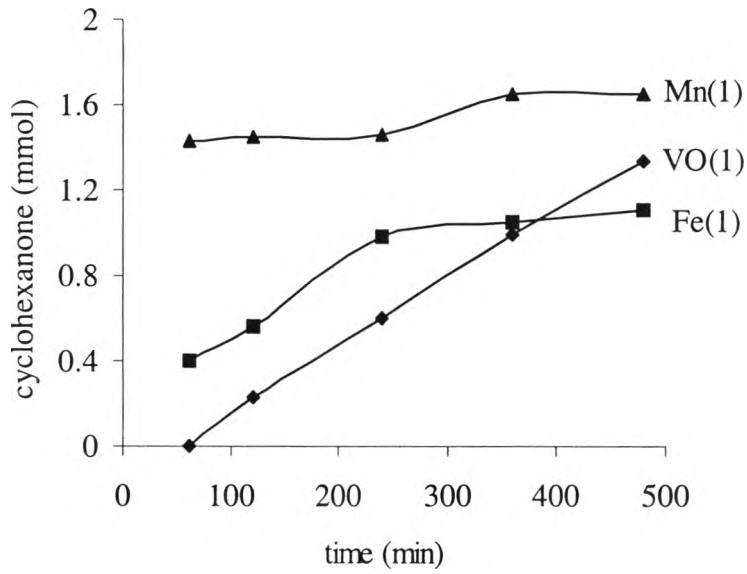

Fig 3.26 Kinetic study on cyclohexane oxidation catalyzed by various catalysts

From Fig 3.26, it was found that complexes **9, 10** and **12** provided an increased amount of cyclohexanone when the reaction time was progressed. Considering complexes **9** and **10**, the amount of cyclohexanone was stable at 6 h, while complexes **12** gave the amount of cyclohexanone increased continuously. It was found that complexes **9, 10** and **12** have a half-life less than 60 min, about 150 min and about 270 min, respectively. This information clearly reinforced the concept of metal dependence in catalyst of the functionalization of hydrocarbons.

3.7.2 Kinetic study of cyclohexane oxidation examined by cyclic voltammetry

The kinetic study of cyclohexane oxidation using complexes **9, 10** and **12** as catalyst and TBHP as oxidant were examined by cyclic voltammetry. The kinetic voltammogram results are presented in Figs 3.27 - 3.29.

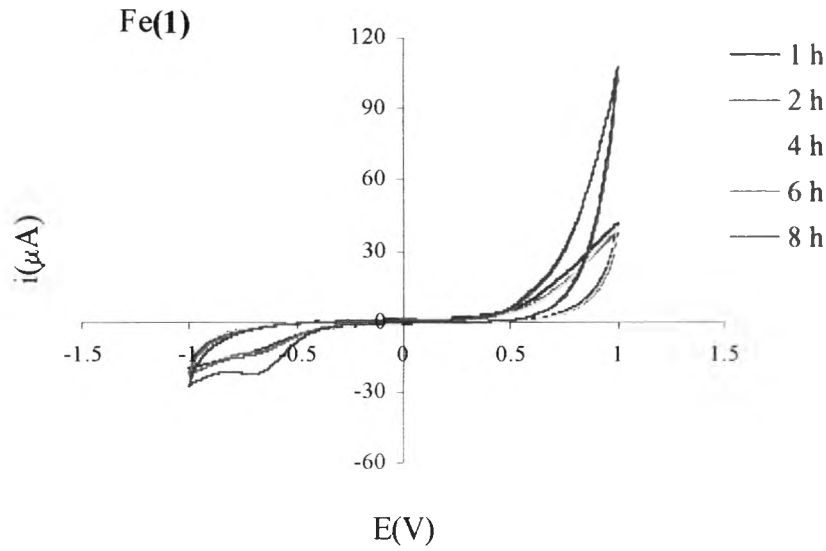

Fig 3.27 Kinetic cyclic voltammogram of cyclohexane oxidation catalyzed by complex **9** in 0.1 M $C_{16}H_{36}FNP$ obtained from using glassy carbon electrode as a working electrode, scan rate: 0.05 V/s

From Fig 3.27, complex **9** did not show redox reaction during 1 to 4 h, but display irreversible reduction at a potential -0.70 V versus silver wire at 6 and 8 h.

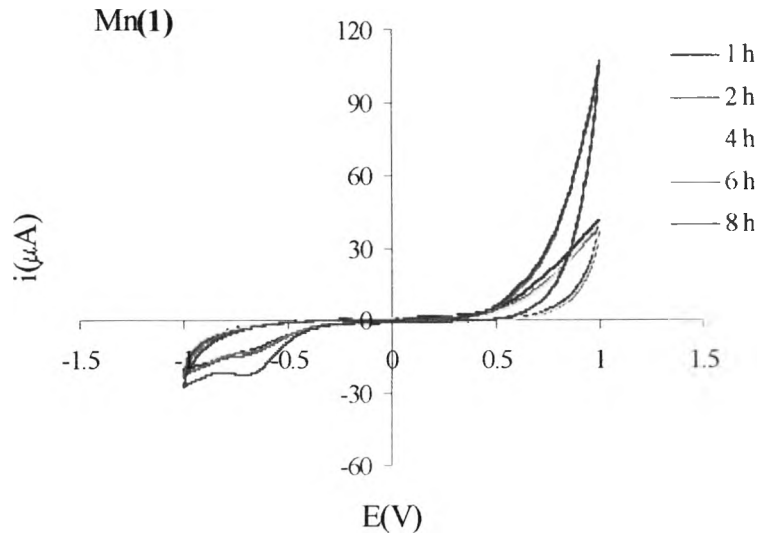

Fig 3.28 Kinetic cyclic voltammogram of cyclohexane oxidation catalyzed by complex **10** in 0.1 M $C_{16}H_{36}FNP$ obtained from using glassy carbon electrode as a working electrode, scan rate: 0.05 V/s

From Fig 3.28, complex **10** did not show redox reaction during 1 to 4 h, but displayed irreversible reduction at a potential -0.70 V versus silver wire at 6 and 8 h.

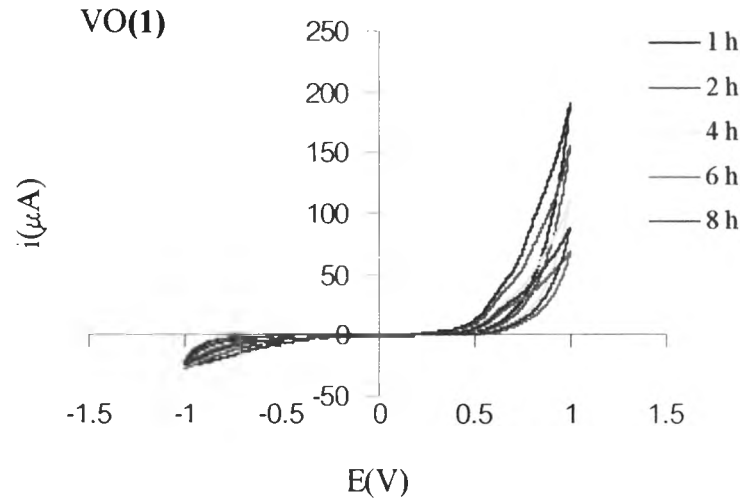

Fig 3.30 Kinetic cyclic voltammogram of cyclohexane oxidation catalyzed by complex **12** in 0.1 M $C_{16}H_{36}FNP$ obtained from using glassy carbon electrode as a working electrode, scan rate: 0.05 V/s

From Fig 3.29, complex **12** did not show redox reaction during 1 to 8 h.

From Figs 3.27-3.29, it was found that complexes **9** and **10** did not show redox reaction during 1 to 4 h, but showed irreversible reaction at 6 and 8 h while complex **12** did not reveal redox reaction during 1 to 8 h. This result could be implied that complexes **9** and **10** had an interaction with TBHP to gain a high valent oxidizing agent (LM^{III}-OO^tBu)[38] during 1 to 4 h; thus these complexes did not show redox reaction during 1 to 4 h. At 6 and 8 h, the oxidation of cyclohexane was nearly completed about 6 h; thus complexes **9** and **10** displayed irreversible reaction. The cyclohexane oxidation catalyzed by complex **12** did not complete during 8 h. This

implied complex **12** may be form of (LM^{III}-OO^{t}Bu). Thus, complexes **12** did not display redox reaction during 1 to 8 h.

3.8 Analysis of oxidizing power in cyclohexane oxidation

The amount of oxidizing agent used in cyclohexane oxidation was followed using iodometric titration. In this experiment, H_2O_2 was used as an oxidizing agent in cyclohexane oxidation catalyzed by metal Schiff base complexes **9**, **10** and **12**. The results are presented in Table 3.6 and Figs 3.30 - 3.32.

Table 3.6 Kinetic study of cyclohexane oxidation using H_2O_2 as oxidant

Time (min)	**9**		**10**		**12**	
	-one (mmol)	H_2O_2 (mmol)	-one (mmol)	H_2O_2 (mmol)	-one (mmol)	H_2O_2 (mmol)
0	0	14.478	0	14.513	trace	14.541
60	0.521	11.342	0.060	11.538	trace	11.212
120	0.988	9.256	0.078	10.365	trace	10.234
240	1.102	8.409	0.080	8.800	trace	8.605
360	1.160	7.105	0.082	8.148	trace	7.627
480	1.185	6.584	0.085	7.562	trace	6.845

Reaction conditions: cyclohexane (30 mmol), catalyst (0.25 mmol), pyridine and acetonitrile (1:1 V/V) (28 mL), hydrogen peroxide (15 mmol) at RT

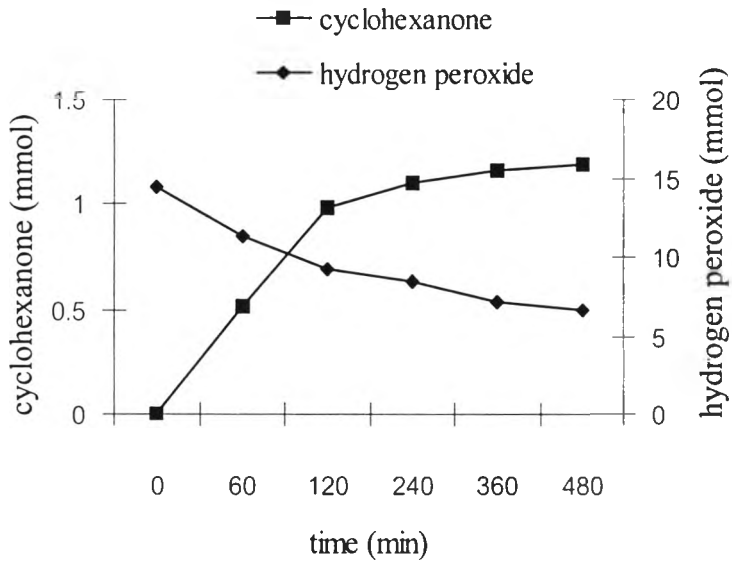

Fig 3.30 Amount of cyclohexanone and hydrogen peroxide left in the reaction catalyzed by complex **9**

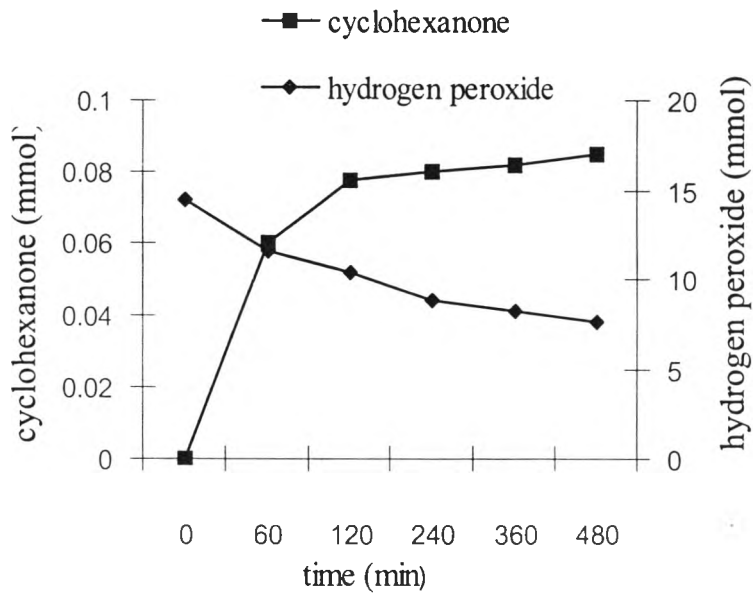

Fig 3.31 Amount of cyclohexanone and hydrogen peroxide left in the reaction catalyzed by complex **10**

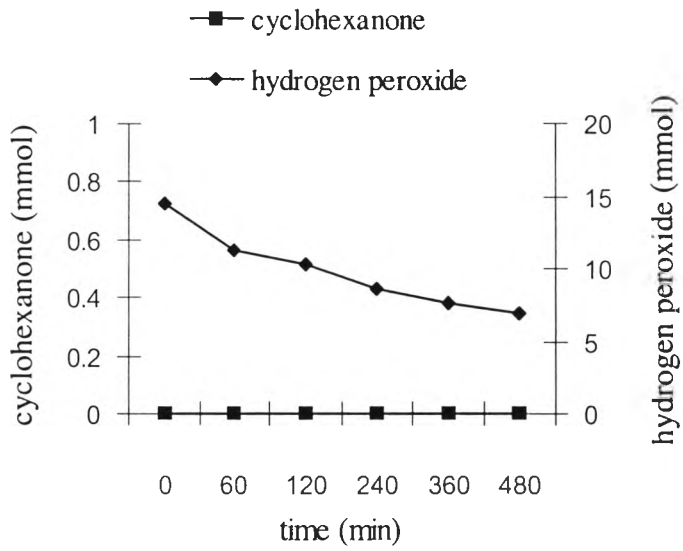

Fig 3.32 Amount of cyclohexanone and hydrogen peroxide left in the reaction catalyzed by complex **12**

From Table 3.8 and Figs 3.30 - 3.32, it could clearly be seen that when the reaction time progressed, complexes **9** and **10** produced certain amount of cyclohexanone while the amount of H_2O_2 in reaction was lessen. The declined amount of H_2O_2 was found to be in proportion to the amount of cyclohexanone produced. In the case of complex **12**, only trace amount of cyclohexanone formed whereas amount of H_2O_2 was decreased. This firmly pointed out that complex **12** did not behave as a good catalyst for alkane oxidation using H_2O_2 as oxidant.

3.9 Oxidation reaction of other organic compounds

The oxidation of cyclohexanol and cyclohexene were investigated using metal Schiff base namely **9, 10** and **12** as catalyst.

3.9.1 Oxidation reaction of cyclohexanol

The oxidation of cyclohexanol using complexes **9, 10** and **12** as catalyst and both H_2O_2 and TBHP as oxidant was investigated. The results are presented in Table 3.7.

Table 3.7 The cyclohexanol oxidation catalyzed by complexes **9, 10** and **12** at 24 h

Catalysts	-one (mmol)	
	H_2O_2	TBHP
9	1.055	9.832
10	0.807	9.663
12	0.560	5.723

Reaction conditions: cyclohexanol (30 mmol), catalyst (0.25 mmol), pyridine and acetonitrile (1:1 V/V) (28 mL), H_2O_2 (15 mmol) at RT or TBHP (15 mmol) at 50 °C.

From Table 3.7, it was found that cyclohexanone was produced as a major product. The functionalization of cyclohexanol tocyclohexanone was found to take place easier than that of cyclohexane. In addition, TBHP also gave better yield than H_2O_2. This result demonstrated that metal Schiff base complexes which showed reversible and quasi-reversible reactions also had a tendency to provide good results in the oxidation of cyclohexanol.

3.9.2 Oxidation reaction of cyclohexene

The oxidation of cyclohexene using complexes **9, 10** and **12** as catalyst and both H_2O_2 and TBHP as oxidant was investigated. The results are presented in Table 3.8.

Table 3.8 The cyclohexene oxidation catalyzed by complexes **9, 10** and **12**

Catalysts	H_2O_2				TBHP			
	2 h		24 h		2 h		24 h	
	-oxide (mmol)	-one (mmol)	-oxide (mmol)	-one (mmol)	-oxide (mmol)	-one (mmol)	-oxide (mmol)	-one (mmol)
9	0.371	0.631	0.424	0.782	0.426	0.871	0.529	0.971
10	0.186	0.576	0.312	0.737	0.371	0.827	0.489	0.955
12	0.152	0.502	0.211	0.627	0.358	0.616	0.262	0.774

Reaction conditions: cyclohexene (30 mmol), catalyst (0.25 mmol), pyridine and acetonitrile (1:1 V/V) (28 mL), H_2O_2 (15 mmol) at RT or TBHP (15 mmol) at 50 °C

From Table 3.8, it was found that cyclohexenone was produced as a major product while cyclohexeneoxide being a minor and cyclohexenol did not occur. This result was different from the previous epoxidation of cyclohexene reported.[39] This outcome demonstrated that metal Schiff base complexes which showed reversible and quasi-reversible reactions provided good results in the oxidation of cyclohexene.